

Temperature effect on wireless impedance monitoring in tendon anchorage of prestressed concrete girder

Jae-Hyung Park^a, Thanh-Canh Huynh^b and Jeong-Tae Kim*

Department of Ocean Engineering, Pukyong National University, 599-1 Daeyeon 3-dong, Nam-gu, Busan 608-737, Republic of Korea

(Received November 4, 2014, Revised January 10, 2015, Accepted January 20, 2015)

Abstract. In this study, the effect of temperature variation on the wireless impedance monitoring is analyzed for the tendon-anchorage connection of the prestressed concrete girder. Firstly, three impedance features, which are peak frequency, root mean square deviation (RMSD) index, and correlation coefficient (CC) index, are selected to estimate the effects of temperature variation and prestress-loss on impedance signatures. Secondly, wireless impedance tests are performed on the tendon-anchorage connection for which a series of temperature variation and prestress-loss events are simulated. Thirdly, the effect of temperature variation on impedance signatures measured from the tendon-anchorage connection is estimated by the three impedance features. Finally, the effect of prestress-loss on impedance signatures is also estimated by the three impedance features. The relative effects of temperature variation and prestress-loss are comparatively examined.

Keywords: temperature effect; wireless monitoring; electro-mechanical impedance; impedance-based; prestress-loss; tendon-anchorage connection; prestressed concrete girder

1. Introduction

Steel tendon is an important component of prestressed concrete (PSC) girder. With prestressing techniques, PSC girders can be larger and even slimmer to be implemented for long-span bridges. However, risks can be worse due to the dependency of the techniques. Among several damage types in the PSC girders, the loss of prestress forces occurs in the tendon anchorage system due to the relaxation of cable stress, the failure of connection components, etc. The loss of prestress forces could lead to the failure of cables and also result in the significant reduction of load carrying capacity and even the collapse of structure. Therefore, damage monitoring in the tendon anchorage system is an important issue.

Up to date, many studies have been focused on damage monitoring in structural connections by using local impedance properties. As the local dynamic characteristics, the method utilizes electro-mechanical (EM) impedance of a coupled PZT (Lead ZirconateTitanate) -structure system

*Corresponding author, Professor, E-mail: idis@pknu.ac.kr

^aBK21Plus Visiting Professor, E-mail: cross96@gmail.com

^bPh.D. Student, E-mail: ce.huynh@gmail.com

to detect the incipient change in structural characteristics at local critical region. The impedance-based method was first proposed by Liang *et al.* (1994). Since then, many researchers have improved the method and have applied the method as a promising way to various damage detection problems (Sun *et al.* 1995, Park *et al.* 2001, Zagrai and Giurgiutiu 2001, Fasel *et al.* 2005, Mascarenas 2006, and Kim *et al.* 2006, Providakis *et al.* 2014, Li *et al.* 2014).

Recently, Kim *et al.* (2010) has applied the impedance-based method for monitoring prestress-loss in PSC bridges by detecting the change in impedance responses at the tendon-anchorage connection. Nguyen and Kim (2012) presented a wireless impedance sensor and a PZT interface technique for impedance monitoring in the tendon-anchorage connection. Also, Huynh and Kim (2014) proposed an analytical model for impedance-based prestress-loss monitoring in tendon anchorage systems. By adopting the wireless sensor and the PZT interface, the automated and cost-efficient operation can be implemented by embedded software for real applications (Lynch *et al.* 2006, Rice *et al.* 2010, Kim *et al.* 2014); however, this fact also leads a very important issue to be solved before real ambient applications. That is temperature-induced change in impedance signature.

Researchers have worked on examining the effect of temperature variation on structural dynamic properties that are utilized for structural health monitoring (Kim *et al.* 2003, Ko and Ni 2005, Kim *et al.* 2007, Xia *et al.* 2006, Sohn 2007, Balmes *et al.* 2009, Xu *et al.* 2010). Temperature-driven variability of local dynamic responses should also be quantified in the determination of impedance features that are used for damage monitoring (Koo *et al.* 2009, Hong *et al.* 2011). Boundary conditions and material constants of both sensor materials and structures are temperature-dependent. The effect of temperature variation should be analyzed in measurement of impedance signatures, extraction of impedance features (e.g., peak frequency), and determination of damage locations and severities. Therefore, it is very important to discriminate the temperature-driven effect on the impedance features extracted from damaged states.

In this study, the effect of temperature variation on the wireless impedance monitoring is analyzed for the tendon-anchorage connection of the prestressed concrete girder. Firstly, three impedance features, which are peak frequency, root mean square deviation (RMSD) index, and correlation coefficient (CC) index, are selected to estimate the effects of temperature variation and prestress-loss on impedance signatures. Secondly, wireless impedance tests are performed on the tendon-anchorage connection for which a series of temperature variation and prestress-loss events are simulated. Thirdly, the effect of temperature variation on impedance signatures measured from the tendon-anchorage connection is estimated by the three impedance features. Finally, the effect of prestress-loss on impedance signatures is also estimated by the three impedance features. The relative effects of temperature variation and prestress-loss are comparatively examined.

2. Impedance features for estimation of temperature effect

2.1 Electro-mechanical impedance

As shown in Fig. 1, an input harmonic voltage $V(\omega)$ induces a deformation of a piezoelectric material (e.g., PZT) due to inverse piezoelectric effect. The PZT patch is surface-bonded to the structure and a force $F(\omega)$ against the deformation is induced into the structure. For 1-*dof* system, the structural mechanical (SM) impedance of the host structure is obtained by the ratio of force

$F(\omega)$ to velocity $\dot{u}(\omega)$ as follows (Liang *et al.* 1994)

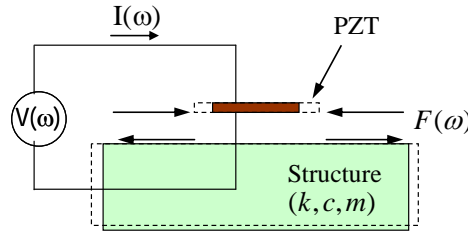


Fig. 1 Coupling interaction between PZT and structure (Huynh and Kim 2014)

$$Z_s(\omega) = \frac{F(\omega)}{\dot{u}(\omega)} = c + m \frac{\omega^2 - \omega_n^2}{\omega} i \tag{1}$$

where c and m are the damping coefficient and the mass of the structure, respectively; ω_n is the angular natural frequency of the structure; and ω is the angular frequency of the excitation voltage. As shown in Eq. (1), SM impedance is a function of mass, damping, and stiffness (i.e., stiffness is introduced from natural frequency, $k = m\omega_n^2$). Thus, the change in structural parameters caused by environmental conditions and damage such as temperature and prestress-loss can be represented by the change in SM impedance.

The EM impedance, $Z(\omega)$, is a combining function of the mechanical impedance of the host structure, $Z_s(\omega)$, and that of the piezoelectric patch, $Z_a(\omega)$. Therefore, the change in structural parameters (i.e., k , m , and c) can be represented by the change in EM impedance. In practice, the electric current $I(\omega)$ is measured and then it is utilized to calculate EM impedance as follows (Liang *et al.* 1994)

$$Z(\omega) = \frac{V}{I} = \left\{ i\omega \frac{w_a l_a}{t_a} \left[\hat{\epsilon}_{33}^T - \frac{1}{Z_a(\omega)/Z_s(\omega) + 1} d_{3x}^2 \hat{Y}_{xx}^E \right] \right\}^{-1} \tag{2}$$

where $\hat{Y}_{xx}^E = (1 + i\eta)Y_{xx}^E$ is the complex Young's modulus of the PZT patch at zero electric field; $\hat{\epsilon}_{xx}^T = (1 - i\delta)\epsilon_{xx}^T$ is the complex dielectric constant at zero stress; d_{3x} is the piezoelectric coupling constant in x -direction at zero stress; and w_a , l_a and t_a are the width, length, and thickness of the piezoelectric transducer, respectively. The parameters η and δ are structural damping loss factor and dielectric loss factor of piezoelectric material, respectively. If excitation frequency is identical to resonant frequency of structure (i.e., $\omega = \bar{\omega}$), the term $Z_a(\omega)/Z_s(\omega)$ is activated in Eq. (1). Then SM impedance takes only the term of damping coefficient (i.e., $Z_s(\omega) = c$). Consequently, the SM impedance for that frequency is comparable with mechanical impedance of the PZT, and EM impedance is expressed as (Nguyen *et al.* 2012)

$$Z(\omega) = \left\{ i\omega \frac{w_a l_a}{t_a} \left[\varepsilon_{33}^T - \frac{1}{Z_a/c + 1} d_{3x}^2 \hat{y}_{xx}^E \right] \right\}^{-1} \quad (3)$$

In Eq. (3), the contribution of SM impedance to EM impedance is the damping coefficient c , which represents not only modal damping but also natural frequency of the structure. Therefore, structural change could be identified sensitively by the change in EM impedance at the resonant frequency.

2.2 Impedance features

For damage characterization, damage indices such as peak frequency, RMSD and CC have been widely used for quantifying the variation of EM impedance signatures. In general, the RMSD index and the CC index exhibit in different natures. The CC index is more sensitive to the horizontal shift (i.e., frequency shift) and less sensitive to the vertical shift (i.e., amplitude shift) of the impedance signatures; meanwhile, the RMSD index is sensitive to both. Previous experimental studies report that the temperature change causes not only the frequency shift but also the amplitude shift of the impedance response (Park *et al.* 1999, Koo *et al.* 2009, and Fabricio *et al.* 2014). To estimate the effect of temperature variation in the tendon anchorage of the PSC girder, therefore, three types of impedance features are selected as follows: change in peak frequency, RMSD, and CC of impedance response. The impedance features are extracted from the impedance response measured from the structure. For each impedance feature, the effect of temperature is estimated by regression analysis.

Firstly, the change in peak frequencies, $\delta\bar{\omega}$, gives the estimation of the change in EM impedance as follows

$$\delta\bar{\omega} = \bar{\omega}_0 - \bar{\omega}_d \quad (4)$$

in which $\bar{\omega}_0$ is the baseline peak frequency of the reference state and $\bar{\omega}_d$ is the corresponding peak frequency of the deviated state (e.g., damaged state).

Secondly, RMSD index is utilized to quantify the change in impedance. The RMSD index is calculated as (Sun *et al.* 1995)

$$RMSD(Z, Z^*) = \sqrt{\frac{\sum_{i=1}^N [Z^*(\omega_i) - Z(\omega_i)]^2}{\sum_{i=1}^N [Z(\omega_i)]^2}} \quad (5)$$

in which $Z(\omega_i)$ is the impedance signature measured for the i^{th} frequency at the reference state and $Z^*(\omega_i)$ is the corresponding impedance signature measured at the special event; and N denotes the number of frequency points in the sweep. Note that the asterisk (*) denotes the special event. Ideally, the RMSD is equal to 0 if the two events are identical and there is no structural change. Otherwise, the RMSD is larger than 0.

Thirdly, CC index can also be used to quantify the change of the whole impedance signatures (Zagrai and Giurgiutiu 2001). The CC index is calculated as follows

$$CC = \frac{1}{\sigma_Z \sigma_{Z^*}} E \left\{ \left[\Im(Z_i) - \Re(\bar{Z}) \right] \left[\Re(Z_i^*) - \Re(\bar{Z}^*) \right] \right\} \quad (6)$$

where $E[.]$ is the expectation operation; $\text{Re}(Z_i)$ and $\text{Re}(Z_i^*)$ represent, respectively, the real parts of the EM impedances measured for the i^{th} frequency before and after the special event; $\text{Re}(\bar{Z})$ and $\text{Re}(\bar{Z}^*)$ signify, respectively, the mean values of impedance signatures (real part) before and after the special event; and σ_Z and σ_Z^* signify, respectively, the standard deviation values of impedance signatures before and after the special event.

Regression analysis gives the information on the relationship between a response variable and one or more independent variables. The relationship obtained from regression analysis can be used to predict values of the response variable and identify variables that most affect the response. The value of each predictor variable can be accessed through statistical tests on the estimated coefficients of the predictor variables. In this study, the polynomial regression model (Devore 1987) is selected from preliminary tests. The n^{th} degree polynomial regression fits the nonlinear relationship between the independent variable and the dependent variable. The polynomial regression model between variables x and Y can be written as

$$Y = \beta_0 + \beta_1 x + \beta_2 x^2 + \dots + \beta_k x^k + \varepsilon \quad (7)$$

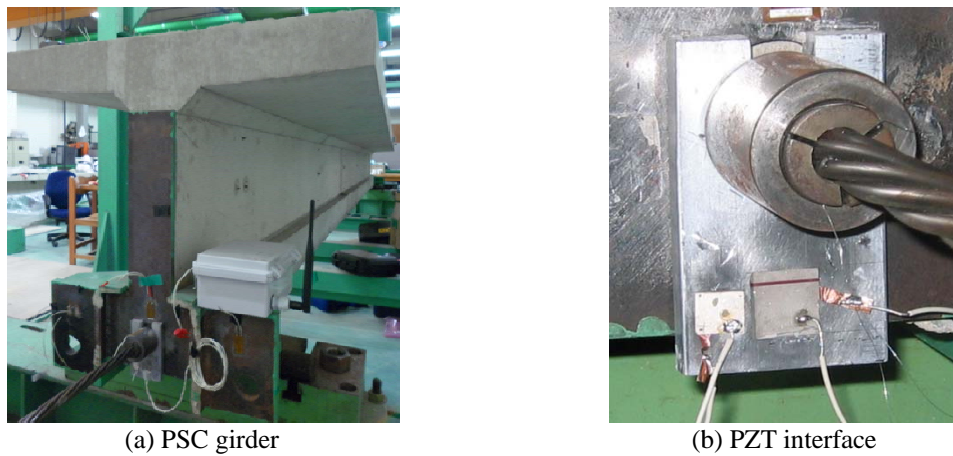
in which ε is a random error variable; and $\beta_0, \beta_1, \beta_2, \dots, \beta_k$ are regression coefficients which are unknown impedance properties.

3. Experiments on tendon-anchorage of PSC girder

3.1 Description of wireless impedance test set-up

As illustrated in Fig. 2(a), impedance tests were performed on a lab-scaled PSC girder. The PSC girder was simply supported and installed on a rigid testing frame. Two simple supports were modeled by steel rods between the girder and the rigid frame. A cable in length of 6.4 m was anchored by two bearing plates at two ends. Tension force was introduced into the cable by a stressing jack. A load cell was installed at one cable anchorage to measure the actual cable force. As detailed in existing publications (Kim *et al.* 2009, Ho *et al.* 2012), the PSC girder model has the T-section reinforced in both longitudinal and transverse direction with 10 mm diameter reinforcing bars. As the prestressing tendon, a seven-wire mono-strand with 15.2 mm diameter was embedded in a 25 mm diameter duct. The baseline prestress force was set to 98.0 kN during the tests.

As shown in Fig. 2(b), an aluminum PZT-interface with a PZT-5A patch (Lead Zirconate Titanate) was installed to the tendon-anchorage connection of the PSC girder. Note that the PZT interface was detailed in Nguyen *et al.* (2012). Impedance signatures of the PZT-interface were measured by an impedance sensor node Imote2/SSeL-I16 (Kim *et al.* 2011, Nguyen *et al.* 2012) placed near the anchorage system. The PZT sensor was excited by a harmonic excitation voltage with 1V-amplitude. The wireless impedance sensor was powered by three D-Cell batteries which ensure the power supply for the sensor node during the test. A base station which include an Imote2 associated with an interfacial computer was placed at 5 m distance from the tendon-anchorage connection. Note also that the wireless impedance sensor system was detailed in Nguyen and Kim (2012).



(a) PSC girder

(b) PZT interface

Fig. 2 Impedance test on tendon anchorage of PSC girder

3.2 Simulation of temperature variation and prestress-loss

3.2.1 Temperature variation

Temperature data were measured by using K-type thermocouple wires and KYOWA (EDX-100A) dynamic logger. A series of tests were performed for 9 consecutive days. Fig. 3 shows the time history of measured temperature during the test period. During the tests on the PSC girder, temperatures varied between 5°C and 23°C. Humidity in the laboratory was kept close to 40~45% in order to minimize the effect of humidity variation on the vibration characteristics. Temperature was controlled as designed for the tests by air conditioners and heaters (e.g., heater on and off) (Hong 2011). Vibration tests started at 18:00 hour of January 8 as the laboratory temperature reached up to 23°C. Then the room temperature was controlled to be decreased gradually for the remaining eight days. It is noted that the room temperature changed day and night. During the test period, the prestress force in the tendon-anchorage was kept to the baseline force (98.0 kN).

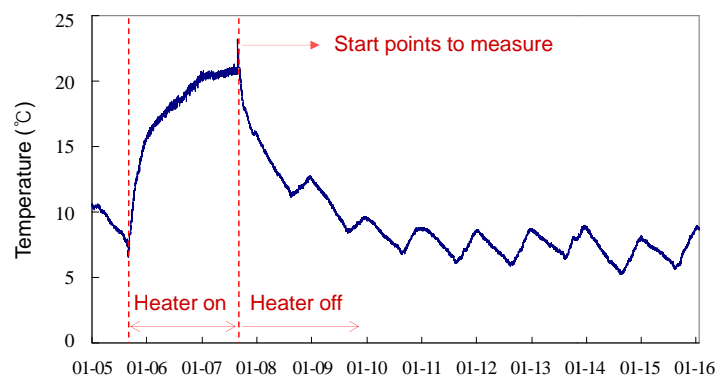


Fig. 3 Time history of measured temperatures from lab-experiment

3.2.2 Damage simulation

While room temperatures were handled to almost constant as 20.5°C, a set of prestress cases were simulated to the PSC girder from which impedance responses were measured from the tendon-anchorage connection. Axial prestress forces were introduced into the tendon by a stressing jack as the tendon was anchored at one end and pulled out at the other. A load cell was installed at the left end to measure the applied prestress force. Each test was conducted after the desired prestress force has been applied and the cable has been anchored. The prestress forces were applied to the test structure up to six different prestress levels (i.e., PS1 – PS6) as listed in Table 1. There were five prestress-loss cases among the six prestress levels.

4. Temperature effects on impedance features

For the temperature variation shown in Fig. 3, impedance signatures were monitored from the tendon-anchorage connection by using the wireless impedance sensor system. Fig. 4(a) shows an impedance signature measured for temperature 20.5°C from the wireless impedance sensor system. A resonant frequency band of 18-20 kHz was taken into account for 501 interval points. Fig. 4(b) shows a series of impedance signatures measured for temperatures 5.4°C ~22.5°C. During the tests, the prestress force was fixed as 98.0 kN (i.e., the prestress-level PS1).

From the figures, the three selected impedance features (i.e., change in peak frequency, RMSD index, and CC index) were used to estimate the effect of temperature variation on the impedance signatures measured from the tendon-anchorage connection of the PSC girder. The overall steps are as follows: firstly, impedance features are extracted for the temperature variation; secondly, time histories of temperatures and impedance features are analyzed; finally, regression analyses are performed by fitting Eq. (7) to estimate polynomial relationships between temperature variation and the extracted impedance features.

4.1 Change in peak frequency versus temperature variation

As the first impedance feature, the change in peak frequency was used to estimate temperature effects on the impedance signatures measured from the tendon-anchorage connection of the PSC girder. As the first and second steps, peak frequencies were extracted from the impedance signatures and changes in peak frequencies were computed by Eq. (4). Fig. 5 show time histories of measured temperatures and extracted peak frequencies for the eight test days. It is observed that the peak frequencies change corresponding to the temperature variation. As the final step, the cubic regression model between the temperature variation and the change in peak frequencies were analyzed as shown in Fig. 6. The empirical equation of the peak frequency (*Freq*) as a function of temperature (*T*) is as follows

$$Freq(kHz) = 3.0 \times 10^{-5} T^3 - 1.0 \times 10^{-3} T^2 + 4.0 \times 10^{-4} T + 19.574 \quad (8)$$

From Eq. (8), it is observed that the peak frequency value changes from 19.56 kHz to 19.45 kHz as temperature (*T*) changes from 5°C to 15°C. This corresponds to 0.55% change in peak frequencies as the temperature shifts to 10°C. It is also noted that the change in peak frequencies with respect to the temperature range above 15°C shows quite nonlinear relationship as it less depends on the temperature change.

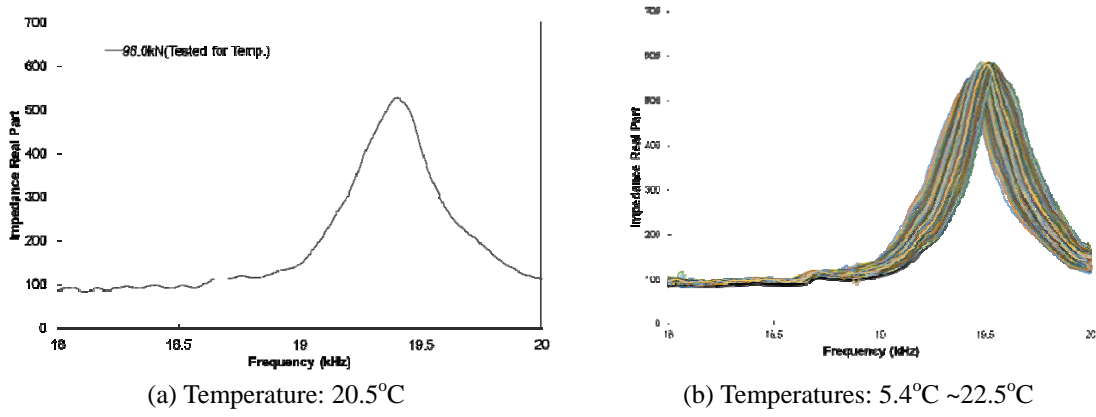


Fig. 4 Impedance signatures from tendon-anchorage connection for temperature variation events

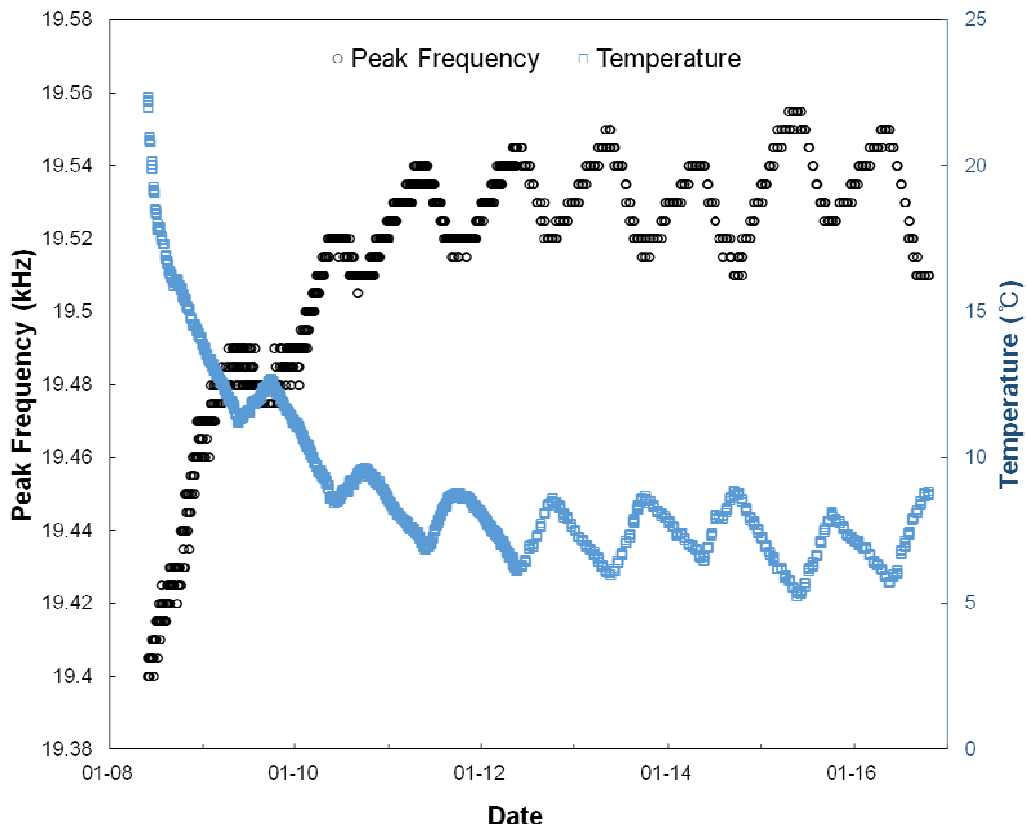


Fig. 5 Time histories of temperatures and extracted peak frequencies

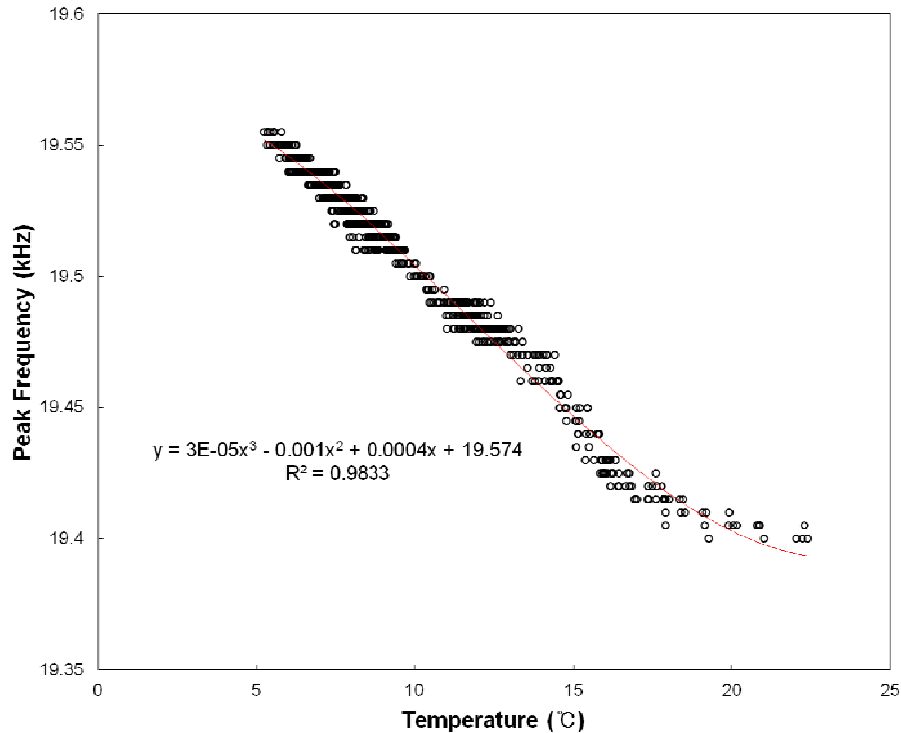


Fig. 6 Cubic regression model between temperature variation and peak frequencies

4.2 RMSD index versus temperature variation

As the second impedance feature, the RMSD index was used to estimate temperature effects on the impedance signatures measured from the tendon-anchorage connection. First, RMSD indices were extracted for the temperature variation by computing Eq. (5). Fig. 7 shows time histories of temperatures and the extracted RMSD indices for the eight test days. It is observed that the RMSD indices change corresponding to the temperature variation. Next, a polynomial regression model was analyzed by fitting Eq. (7). Fig. 8 shows the cubic regression model between the temperature variation and the change in RMSD indices. The empirical equation of the RMSD index ($RMSD$) as a function of temperature (T) is as follows

$$RMSD = 6.0 \times 10^{-5} T^3 - 1.5 \times 10^{-3} T^2 + 3.0 \times 10^{-2} T + 0.7218 \quad (9)$$

From Eq. (9), it is observed that the RMSD indices changes from 0.528 to 0.153 as temperature (T) changes from 5°C to 15°C. This corresponds to 37.5% change in RMSD index as the temperature shifts to 10°C. It is also noted that the RMSD index changes less as the temperature ranges above 15°C due to the nonlinear effect.

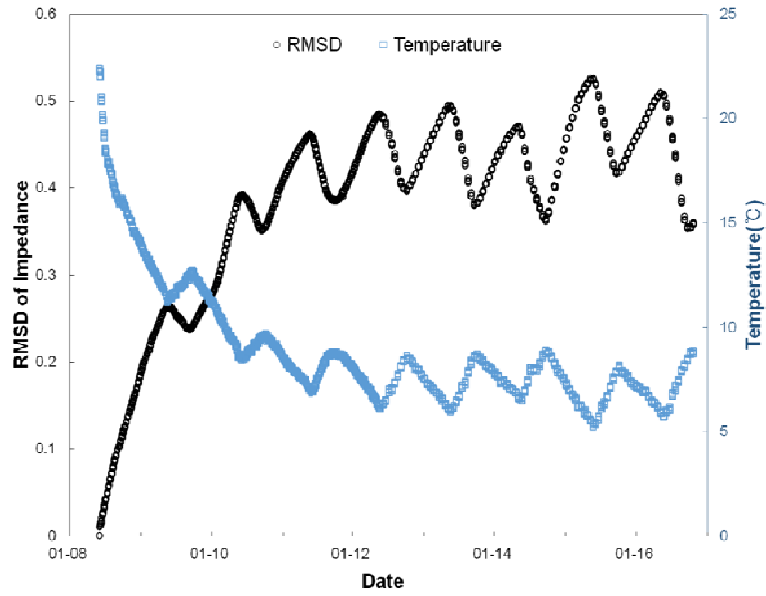


Fig. 7 Time histories of temperatures and RMSD indices

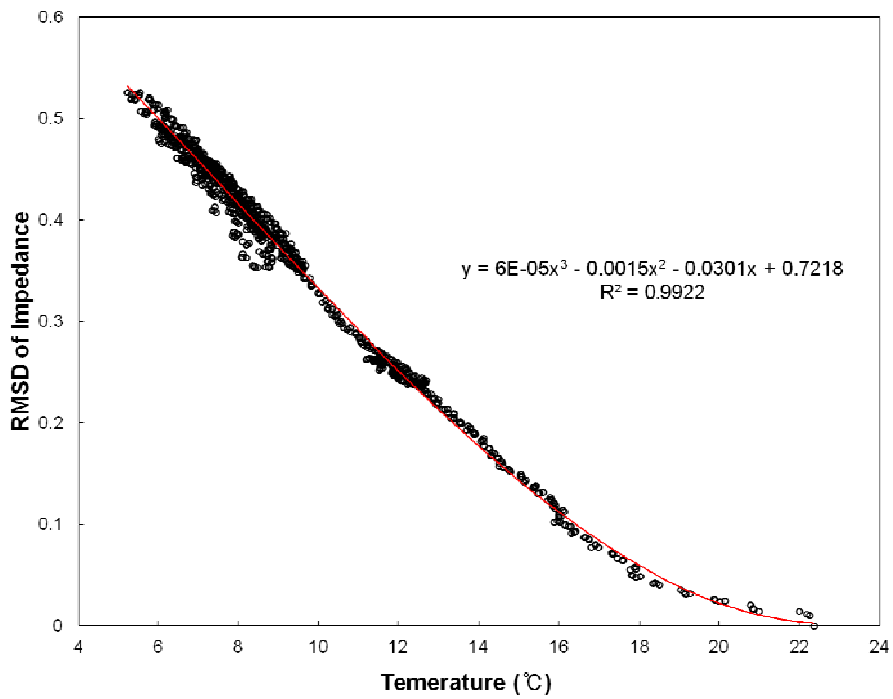


Fig. 8 Cubic regression model between temperature variation and RMSD indices

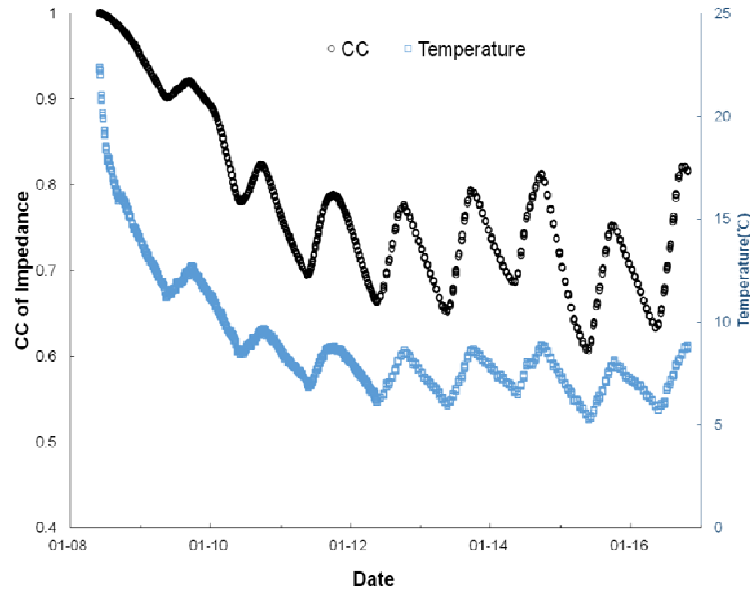


Fig. 9 Time histories of temperatures and CC indices

4.3 CC index versus temperature variation

As the third impedance feature, the CC index was used to estimate temperature effects on the impedance signatures. First, CC indices were extracted for the temperature variation by computing Eq. (6). Fig.9 shows time histories of temperatures and the extracted CC indices for the eight test days. It is observed that the CC indices change corresponding to the temperature variation. Next, a polynomial regression model was analyzed by fitting Eq. (7). Fig. 10 shows the cubic regression model between the temperature variation and the change in CC indices. The empirical equation of the CC index (CC) as a function of temperature (T) is as follows

$$CC = 4.0 \times 10^{-5} T^3 - 4.1 \times 10^{-3} T^2 + 0.1062T + 0.141 \quad (10)$$

From Eq. (10), it is observed that the CC indices change from 0.62 to 0.96 as temperature (T) changes from 5°C to 15°C. This corresponds to 34% change in CC index as the temperature shifts to 10°C. It is also noted that the CC index changes less as the temperature ranges above 15°C due to the nonlinear effect.

5. Temperature effect on impedance-based damage monitoring

For the six prestress-force levels (i.e., PS1 – PS6), as listed in Table 1, impedance signatures were monitored from the tendon-anchorage connection by using the wireless impedance sensor system.

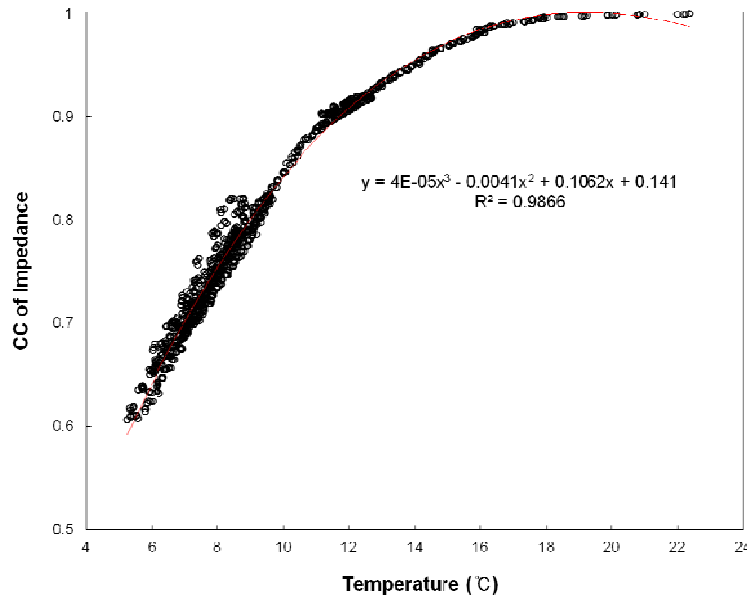


Fig. 10 Cubic regression model between temperature variation and CC indices

Fig. 11 shows the impedance signatures measured for the six prestress-force levels. As the prestress forces decrease from the reference T1 case (98.0 kN), peak frequencies of impedance signatures decrease and their amplitudes also slightly decrease. From Fig. 11, the three types of impedance features (i.e., change in peak frequency, RMSD index, and CC index) were analyzed to examine the damage monitoring results. Then, the relationships between the temperature variation and the impedance features which were analyzed in the previous section were implemented to analyze the effect of temperature variation on the damage monitoring results.

5.1 Damage monitoring by change in peak frequency

Firstly, the relationship between the six prestress-force levels and their corresponding peak frequencies of impedance signatures was estimated as shown in Fig. 12. The shifts in peak frequencies for the five prestress-loss cases (i.e., PS2 - PS6) were estimated as listed in Table 1. A cubic regression curve was fitted to examine the sensitivity of the change in peak frequencies to the change in prestress forces. As the prestress forces decrease by half from 98.0 kN to 49.0 kN, their corresponding peak frequencies decrease from 19.410 kHz to 19.285 kHz, which is about 0.64% decrement. If the forces decrease by 30% from 98.0 kN to 68.6 kN, the corresponding peak frequencies decrease from 19.41 kHz to 19.345 kHz, which is about 0.33% decrement.

Remind from Fig. 6 and Eq. (8) that the peak frequency value changes about 0.055% as the temperature changes about 1°C. Using the selected impedance feature (i.e., the change in peak frequency), therefore, it is estimated that the prestress-force change from 98.0 kN to 49.0 kN may not be detected if the temperature variation is above 12°C. Analogously, the prestress-force shift from 98.0 kN to 68.6 kN may not be detected if the temperature variation is as small as 6°C.

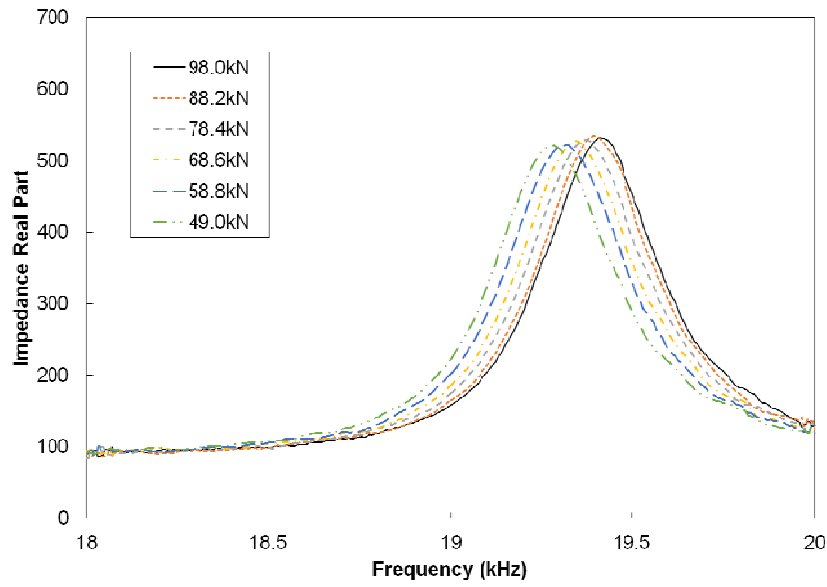


Fig. 11 Impedance signatures measured for six prestress-force levels

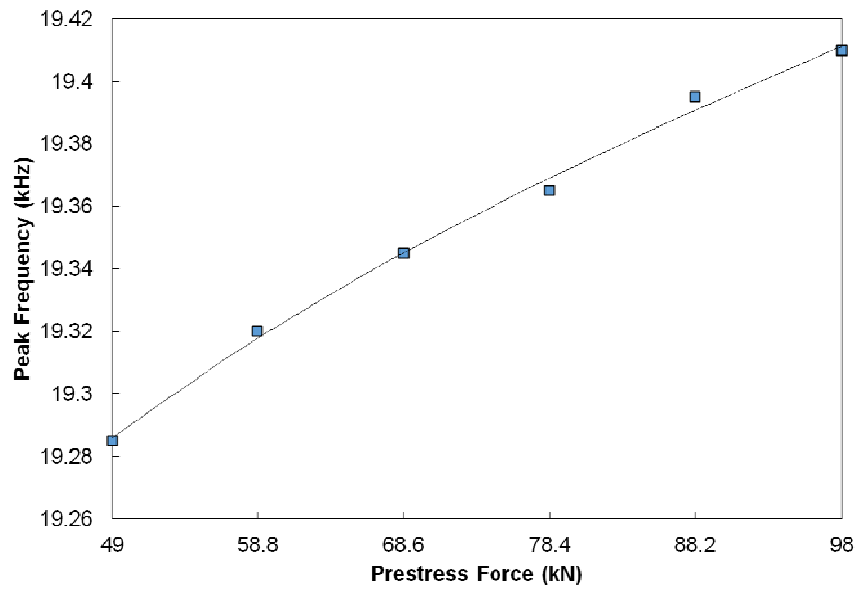


Fig. 12 Peak frequencies of impedance signatures for six prestress-force levels

Table 1 Impedance signatures measured for six prestress levels of PSC girder

Prestress Case	Prestress Force (kN)	Peak Frequency (kN)	Frequency Shift Index (%)	RMSD Index (%)	CC Index (%)
PS 1	98.0	19.410	0.0	0.0	100
PS 2	88.2	19.395	0.08	4.3	99.7
PS 3	78.4	19.365	0.23	11.5	98.0
PS 4	68.6	19.345	0.33	18.4	94.9
PS 5	58.8	19.320	0.46	25.5	90.2
PS 6	49.0	19.285	0.64	34.3	82.4

5.2 Damage monitoring by RMSD index

Secondly, the relationship between the six prestress-force levels and their corresponding RMSD indices was estimated as shown in Fig. 13. The RMSD indices for the six prestress-force levels were estimated as listed in Table 1. A cubic regression curve was fitted to examine the sensitivity of the RMSD indices to the change in prestress forces. As the prestress forces decrease by half from 98.0 kN to 49.0 kN, their corresponding RMSD indices change from 0 to 0.343 (e.g., 34.3% change). If the forces decrease by 30% from 98.0 kN to 68.6 kN, the corresponding RMSD indices change from 0 to 0.184 (e.g., 18.4% change).

Remind from Fig. 7 and Eq. (9) that the RMSD index changes about 3.75% as the temperature changes about 1°C. Using the selected impedance feature (i.e., the RMSD index), therefore, it is estimated that the prestress-force change from 98.0 kN to 49.0 kN may not be detected if the temperature variation is above 9°C. Analogously, the prestress-force shift from 98.0 kN to 68.6 kN may not be detected if the temperature variation is as small as 5°C.

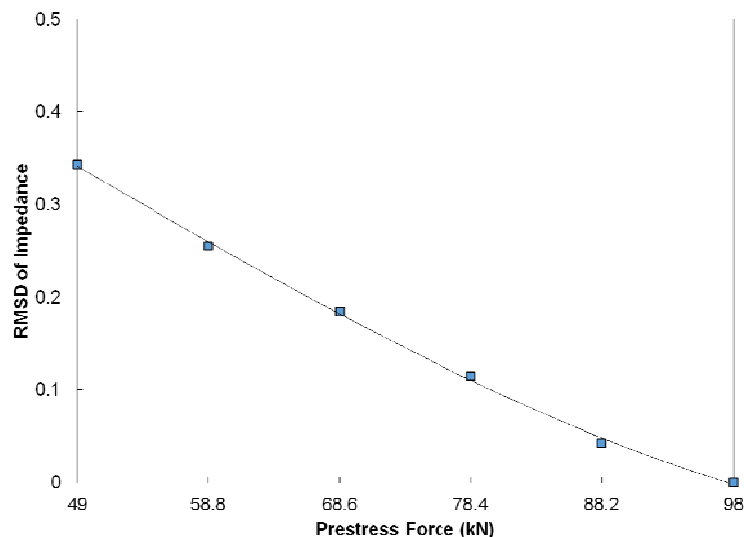


Fig. 13 RMSD indices of impedance signatures for six prestress-force levels

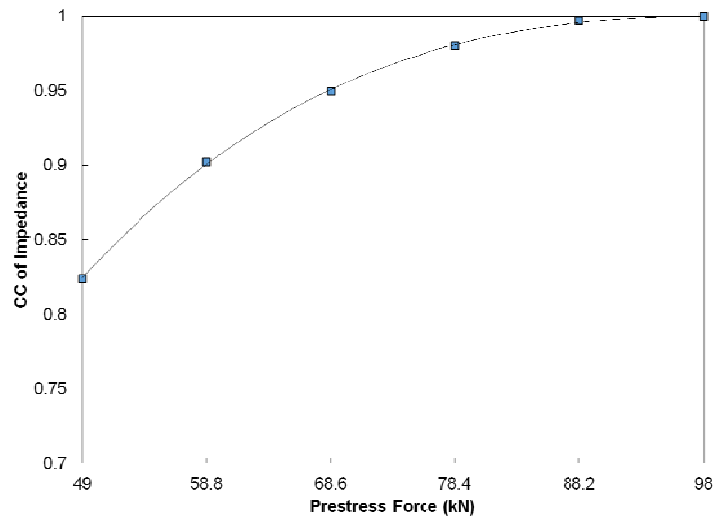


Fig. 14 CC indices of impedance signatures for six prestress-force levels

5.3 Damage monitoring by CC index

Thirdly, the relationship between the six prestress-force levels and their corresponding CC indices was estimated as shown in Fig. 14. The CC indices for the six prestress-force levels were estimated as listed in Table 1. A cubic regression curve was fitted to examine the sensitivity of the CC indices to the change in prestress forces. As the prestress forces decrease by half from 98.0 kN to 49.0 kN, their corresponding CC indices change from 1.0 to 0.824 (e.g., 17.6% change). If the forces decrease by 30% from 98.0 kN to 68.6 kN, the corresponding RMSD indices change from 1.0 to 0.949 (e.g., 5.1% change).

Remind from Fig. 8 and Eq. (10) that the CC index changes about 3.4% as the temperature changes about 1°C. Using the selected impedance feature (i.e., the CC index), therefore, it is estimated that the prestress-force change from 98.0 kN to 49.0 kN may not be detected if the temperature variation is above 5°C. Analogously, the prestress-force shift from 98.0 kN to 68.6 kN may not be detected if the temperature variation is as small as 1.5°C.

6. Conclusions

In this study, the effect of temperature variation on the wireless impedance monitoring was analyzed for the tendon-anchorage connection of the prestressed concrete girder. Firstly, three impedance features (i.e., change in peak frequency, RMSD index, and CC index) were selected to estimate the effects of temperature variation and prestress-loss on impedance signatures. Secondly, wireless impedance tests were performed on the tendon-anchorage connection for which a series of temperature variation and prestress-loss events were simulated. Thirdly, the effect of temperature changes on impedance signatures measured from the tendon-anchorage connection were estimated by the three impedance features. Finally, the effect of prestress-loss on impedance signatures was

estimated by the three impedance features.

By using the three impedance features, temperature effects on impedance signatures measured from the tendon-anchorage connection of the PSC girder were analyzed as follows:

- All selected impedance features were sensitive to the temperature change;
- The relationships between the temperature variation and the impedance features were nonlinear like a set of cubic regression models; and
- The RMSD and CC indices varied much higher than the change in peak frequency under the temperature variation.

By employing the same features, prestress-loss effects on impedance signatures at the tendon-anchorage connection were analyzed as follows:

- All three impedance features varied sensitively with the prestress-loss events;
- The variations of RMSD and CC indices were much more significant than the change in peak frequency under the prestress-loss effects; and
- The change in peak frequency produced the most favorable damage monitoring under the temperature change.

Acknowledgements

This work was supported by Basic Science Research Program through the National Research Foundation of Korea (NRF) funded by the Ministry of Education, Science and Technology (NRF-2013R1A1A2A10012040). The graduate student and BK21Plus professor involved in this research were also partially supported by the Brain Korea 21 Plus program of Korean Government.

References

- Balmes, E., Basseville, M., Mevel, L. and Nasser, H. (2009), "Handling the temperature effect in vibration monitoring of civil structures: A combined subspace-based and nuisance rejection approach", *Control Eng. Pract.*, **17**(1), 80-87.
- Devore, J.L. (1987), *Probability and Statistics for Engineering and the Sciences*, 2nd Ed., Brooks/Cole Publishing Company, Monterey, California.
- Fasel, T.R., Sohn, H., Park, G. and Farrar, C.R. (2005), "Active sensing using impedance-based ARX models and extreme value statistics for damage detection", *Earthq. Eng. Struct. D.*, **34**(7), 763-785.
- Ho, D.D., Kim, J.T., Stubbs, N. and Park, W.S. (2012), "Prestress-force estimation in PSC girder using modal parameters and system identification", *Adv. Struct. Eng.*, **15**(6), 997-1012.
- Hong, D.S. (2011), *Vibration-Impedance-Based Hybrid Structural Health Monitoring and Temperature Effect Assessment in Girder's Structures*, PhD Thesis, Department of Ocean Engineering, Pukyong National University, Korea.
- Huynh, T.C. and Kim, J.T. (2014), "Impedance-based cable force monitoring in tendon-anchorage using portable PZT-interface technique", *Math. Probl. Eng.*, **2014**, Article ID 784731, 11 pages.
- Kim, J.T., Huynh, T.C. and Lee, S.Y. (2014), "Wireless structural health monitoring of stay cables under two consecutive typhoons", *Struct. Monitor. Maint.*, **1**(1), 47-67.
- Kim, J.T., Park, J.H., Hong, D.S., Cho, H.M., Na, W.B. and Yi, J.H. (2006), "Vibration and impedance monitoring for prestress-loss in PSC girder bridges", *Smart Struct. Syst.*, **5**(1), 81-94.
- Kim, J.T., Yun, C.B. and Yi, J.H. (2003), "Temperature effects on frequency-based damage detection in plate-girder bridges", *J. KSCE*, **7**(6), 725-733.
- Kim, J.T., Na, W.B., Park, J.H. and Hong, D.S. (2006), "Hybrid health monitoring of structural joints using

- modal parameters and EMI signatures”, *Proceeding of SPIE*, San Diego, USA.
- Kim, J.T, Park, J.H. and Lee, B.L. (2007), “Vibration-based damage monitoring in model plate-girder bridges under uncertain temperature conditions”, *Eng. Struct.*, **29**(7), 1354-1365.
- Kim, J.T., Park, J.H., Hong, D.S. and Park, W.S. (2010), “Hybrid health monitoring of prestressed concrete girder bridges by sequential vibration-impedance approaches”, *Eng. Struct.*, **32**, 115-128.
- Kim, J.T., Park, J.H., Hong, D.S. and Ho, D.D. (2011), "Hybrid acceleration-impedance sensor nodes on Imote2-platform for damage monitoring in steel girder connections", *Smart Struct. Syst.*, **7**(5), 393-416.
- Ko, J.M. and Ni, Y.Q. (2005), “Technology developments in structural health monitoring of large-scale bridges”, *Eng. Struct.*, **27**, 1715-1725.
- Koo, K.Y., Park, S., Lee, J.J. and Yun, C.B. (2009), “Automated impedance-based structural health monitoring incorporating effective frequency shift for compensating temperature effects”, *J. Intel. Mat. Syst. Str.*, **20**(4), 367-377.
- Li, H.N, Yi, T.H., Ren L., Li, D.S., and Huo, L.S. (2014), “Review on innovations and applications in structural health monitoring for infrastructures”, *Struct. Monitor. Maint.*, **1**(1), 1-45.
- Liang, C., Sun, F.P. and Rogers, C.A. (1994), “Coupled electro-mechanical analysis of adaptive material - Determination of the actuator power consumption and system energy transfer”, *J. Intel. Mat. Syst. Str.*, **5**, 12-20.
- Liang, C., Sun, F.P. and Rogers, C.A. (1996), “Electro-mechanical impedance modeling of active material systems”, *Smart Mat.Struct.*, **5**(2), 171-186.
- Lynch, J.P., Wang, W., Loh, K.J., Yi, J.H. and Yun, C.B. (2006), “Performance monitoring of the Geumdang Bridge using a dense network of high-resolution wireless sensors”, *Smart Mat.Struct.*, **15**(6), 1561-1575.
- Mascarenas, D.L. (2006), *Development of an impedance-based wireless sensor node for monitoring of bolted joint preload*, MS Thesis, Department of Structural Engineering, University of California in San Diego, USA.
- Nguyen, K.D. and Kim, J.T. (2012), “Smart PZT-interface for wireless impedance-based prestress-loss monitoring in tendon-anchorage connection”, *Smart Struct. Syst.*, **9**(6), 489-504.
- Nguyen, K.D., Lee, P.Y. and Kim, J.T. (2012), “Automated monitoring of cable-anchorage force by Imote2-platformed impedance sensor node”, *Adv. Sci. Lett.*, **14**(1), 136-140.
- Park, G., Cudney, H.H. and Inman, D.J. (2001), “Feasibility of using impedance-based damage assessment for pipeline structures”, *Earthq. Eng. Struct. D.*, **30**(10), 1463-1474.
- Providakis, C., Stefanaki, K., Voutetaki, M., Tsompanakis, J. and Stavroulaki, M. (2014), “A near and far-field monitoring technique for damage detection in concrete structures”, *Struct. Monitor.Maint.*, **1**(2), 339-356.
- Rice, J.A., Mechitov, K., Sim, S.H., Nagayama, T., Jang, S., Kim, R., Spencer, Jr, B.F., Agha, G. and Fujino, Y. (2010), “Flexible smart sensor framework for autonomous structural health monitoring”, *Smart Struct. Syst.*, **6**(5-6), 423-438.
- Sohn, H. (2007), “Effects of environmental and operational variability on structural health monitoring”, *Philos. T. R. Soc. A*, **365**, 539-560.
- Sun, F.P., Chaudhry Z., Liang, C. and Rogers C.A. (1995), “Truss structure integrity identification using PZT sensor-actuator”, *J. Intel. Mat. Syst. Str.*, **6**, 134-139.
- Xia, Y., Hao, H., Zanardo, G. and Deeks, A. (2006), “Long term vibration monitoring of an RC slab: temperature and humidity effect”, *Eng. Struct.*, **28**(3), 441-452.
- Xu, Y.L., Chen, B., Ng, C.L., Wong, K.Y. and Chan, W.Y. (2010), “Monitoring temperature effect on a long suspension bridges”, *Struct. Control Health.*, **17**(6), 632-653.
- Zagrai, A.N. and Giurgiutiu, V. (2001), “Electro-mechanical impedance method for crack detection in thin plates”, *J. Intel. Mat. Syst. Str.*, **12**(10), 709-718.